*Geophysical Research Letters*

Supporting Information for

# Magnitude and uncertainty of nitrous oxide emissions from North America based on bottom-up and top-down approaches: Informing future research and national inventories

R. Xu[1,2], H. Tian[1], N. Pan[1], R. L. Thompson[3], J. G. Canadell[4], E. A. Davidson[5], C. Nevison[6], W. Winiwarter[7,8], H. Shi[1], S. Pan[1], J. Chang[9], P. Ciais[10], S. R. S. Dangal[11], A. Ito[12], R. B. Jackson[13], F. Joos[14], R. Lauerwald[15], S. Lienert[14], T. Maavara[16], D. B. Millet[17], P. A. Raymond[16], P. Regnier[18], F. N. Tubiello[19], N. Vuichard[10], K. C. Wells[17], C. Wilson[20,21], J. Yang[22], Y. Yao[1], S. Zaehle[23], F. Zhou[24]

[1]International Center for Climate and Global Change Research, School of Forestry and Wildlife Sciences, Auburn University, Auburn, AL, USA; [2]Forest Ecosystems and Society, Oregon State University, Corvallis, OR, USA; [3]Norsk Institutt for Luftforskning, NILU, Kjeller, Norway; [4]Global Carbon Project, CSIRO Oceans and Atmosphere, Canberra, Australia; [5]Appalachian Laboratory, University of Maryland Center for Environmental Science, Frostburg, MD, USA; [6]University of Colorado Boulder/INSTAAR, Boulder, CO, USA; [7]International Institute for Applied Systems Analysis, Laxenburg, Austria; [8]Institute of Environmental Engineering, University of Zielona Góra, Zielona Góra, Poland; [9]College of Environmental and Resource Sciences, Zhejiang University, Hangzhou, China; [10]Laboratoire des Sciences du Climat et de l'Environnement, LSCE, CEA CNRS, UVSQ UPSACLAY, Gif sur Yvette, France ; [11]School of Natural Resources, University of Nebraska – Lincoln, NE, USA; [12]Earth System Division, National Institute for Environmental Studies, Tsukuba, Japan; [13]Department of Earth System Science, Woods Institute for the Environment, and Precourt Institute for Energy, Stanford University, Stanford, CA, USA; [14]Climate and Environmental Physics, Physics Institute and Oeschger Centre for Climate Change Research, University of Bern, Bern, Switzerland; [15]Université Paris-Saclay, INRAE, AgroParisTech, UMR ECOSYS, Thiverval-Grignon, France; [16]Yale School of the Environment, New Haven, CT, USA; [17]Department of Soil, Water, and Climate, University of Minnesota, MN, USA. [18]Department Geoscience, Environment & Society-BGEOSYS, Université Libre de Bruxelles, Brussels, Belgium; [19]Statistics Division, Food and Agriculture Organization of the United Nations, Via Terme di Caracalla, Rome, Italy; [20]National Centre for Earth Observation, University of Leeds, Leeds, UK; [21]Institute for Climate and Atmospheric Science, School of Earth and Environment, University of Leeds, Leeds, UK; [22]Department of Forestry, Mississippi State University, Mississippi State, MS, USA. [23]Max Planck Institute for Biogeochemistry, Jena, Germany; [24]Sino-France Institute of Earth Systems Science, Laboratory for Earth Surface Processes, College of Urban and Environmental Sciences, Peking University, Beijing, China.

Corresponding author: Hanqin Tian (tianhan@auburn.edu)

**Contents of this file**

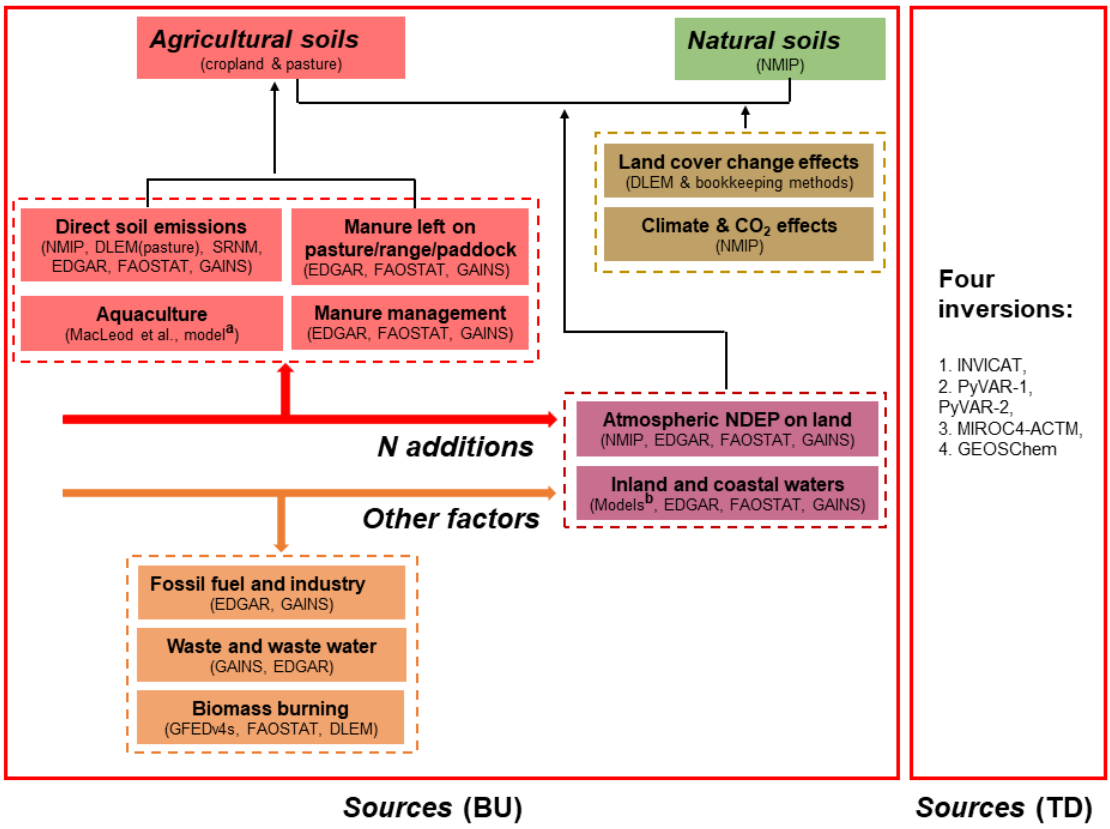


**Figure S1.** The methodology for data synthesis of North American $N_2O$ sources. BU and TD represent bottom-up and top-down methods, respectively. The color codes are the same as that used in Table 1 and Figures. 1–2. We utilize both approaches, including 17 BU and five TD estimates of $N_2O$ fluxes. For sources estimated by BU, we include six process-based terrestrial biosphere modeling studies (Tian et al., 2019); one nutrient budget model (Beusen et al., 2016; Bouwman et al., 2013; Bouwman et al., 2011); one inventory for aquaculture $N_2O$ in 2013 (MacLeod et al., 2019); two inland water modeling studies (Lauerwald et al., 2019; Maavara et al., 2019; Yao et al., 2020); one statistical model SRNM based on spatial extrapolation of field measurements (Wang et al., 2019); and four GHG inventories: EDGAR v4.3.2 (Janssens-Maenhout et al., 2019), FAOSTAT (Tubiello et al., 2015), GAINS (Winiwarter et al., 2018), and GFED4s (Van Der Werf et al., 2017). [a]The nutrient budget model (Beusen et al., 2016; Bouwman et al., 2013; Bouwman et al., 2011) provides N flows in global freshwater and marine aquaculture over the period 1980–2016. [b]Model-based estimates of $N_2O$ emissions from 'Inland and coastal waters' include rivers and reservoirs (Maavara et al., 2019; Yao et al., 2020), lakes (Lauerwald et al., 2019), and estuaries (Maavara et al., 2019).

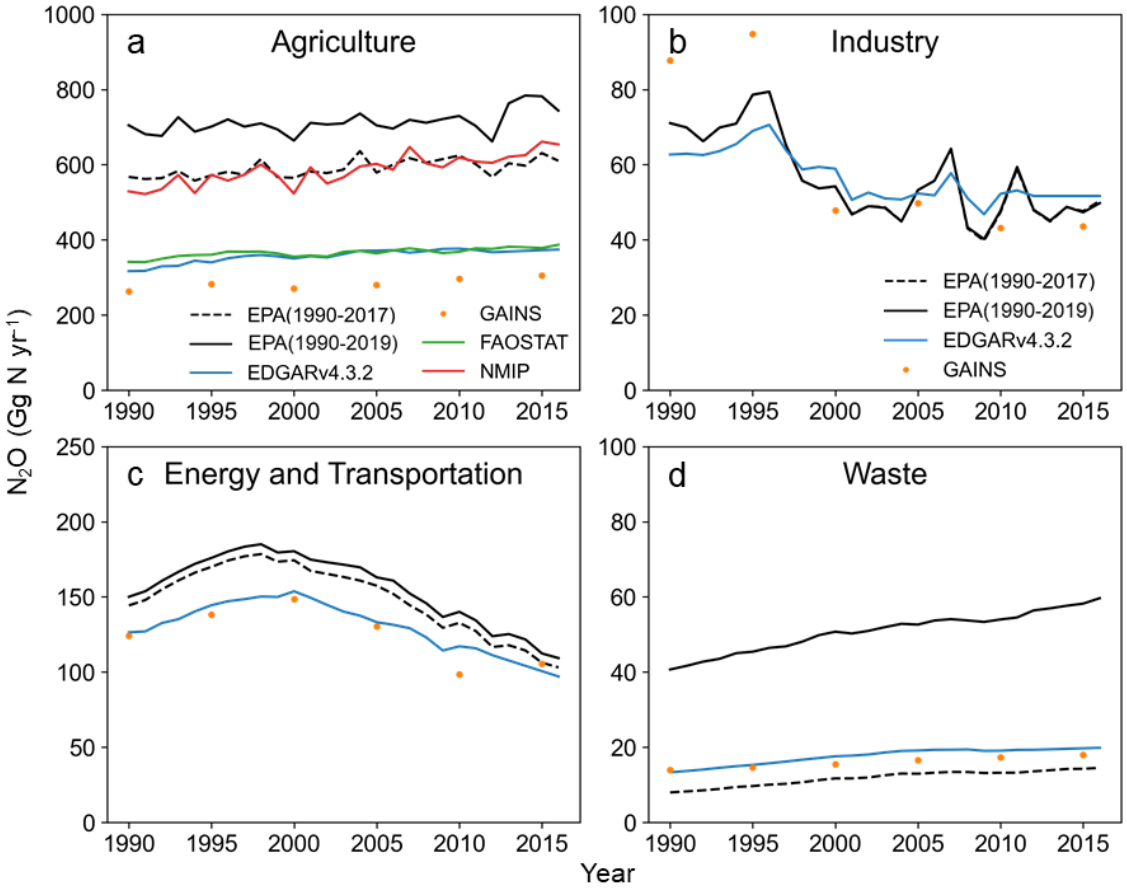


**Figure S2.** Comparison of our BU-estimated anthropogenic $N_2O$ emissions with EPA during 1990–2016 in the U.S. Anthropogenic $N_2O$ sectors include **(a)** agriculture, **(b)** industry, **(c)** energy and transportation, and **(d)** waste. Note: 'NMIP' in **(a)** not only includes the NMIP model results of crop soil emissions and NDEP, but also DLEM-based 'manure left on pasture', model-based indirect emissions from 'inland waters, estuaries, and coastal zones', and 'manure management' based on EDGARv4.3.2 and GAINS.

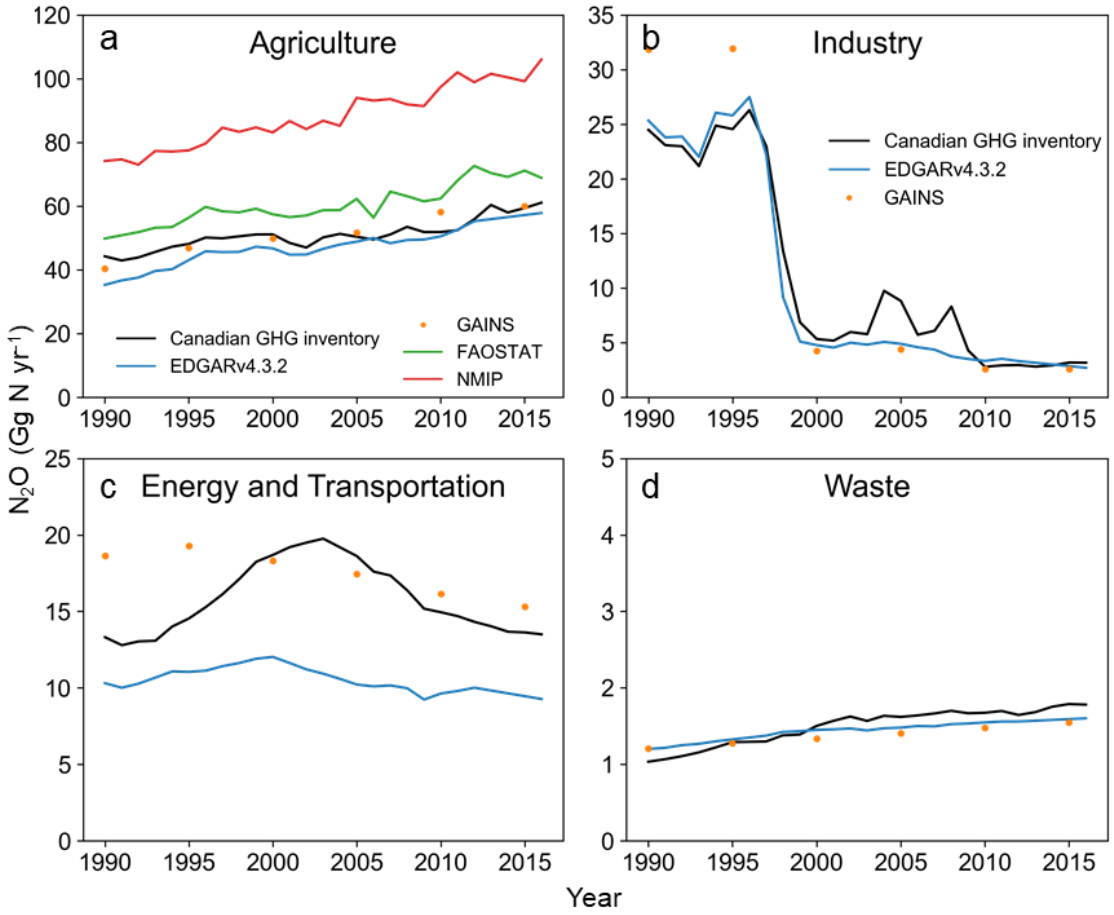


**Figure S3.** Comparison of our BU-estimated anthropogenic $N_2O$ emissions with GHG inventory during 1990–2016 in Canada. Anthropogenic $N_2O$ sectors include **(a)** agriculture, **(b)** industry, **(c)** energy and transportation, and **(d)** waste. Note: 'NMIP' in **(a)** not only includes the NMIP model results of crop soil emissions and NDEP, but also DLEM-based 'manure left on pasture', model-based indirect emissions from 'inland waters, estuaries, and coastal zones', and 'manure management' based on EDGARv4.3.2 and GAINS.

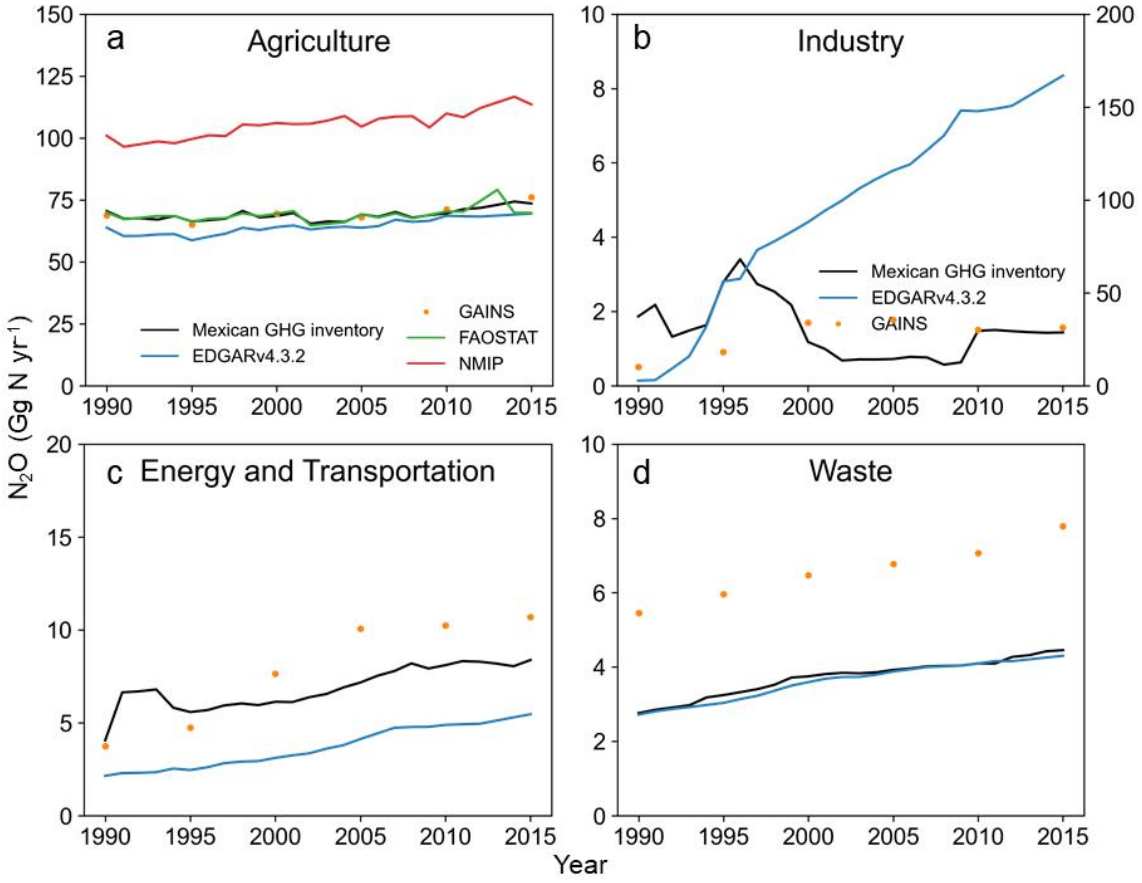


**Figure S4.** Comparison of our BU-estimated anthropogenic $N_2O$ emissions with GHG inventory during 1990–2015 in Mexico. Anthropogenic $N_2O$ sectors include **(a)** agriculture, **(b)** industry, **(c)** energy and transportation, and **(d)** waste. Note: 'NMIP' in **(a)** not only includes the NMIP model results of crop soil emissions and NDEP, but also DLEM-based 'manure left on pasture', model-based indirect emissions from 'inland waters, estuaries, and coastal zones', and 'manure management' based on EDGARv4.3.2 and GAINS.

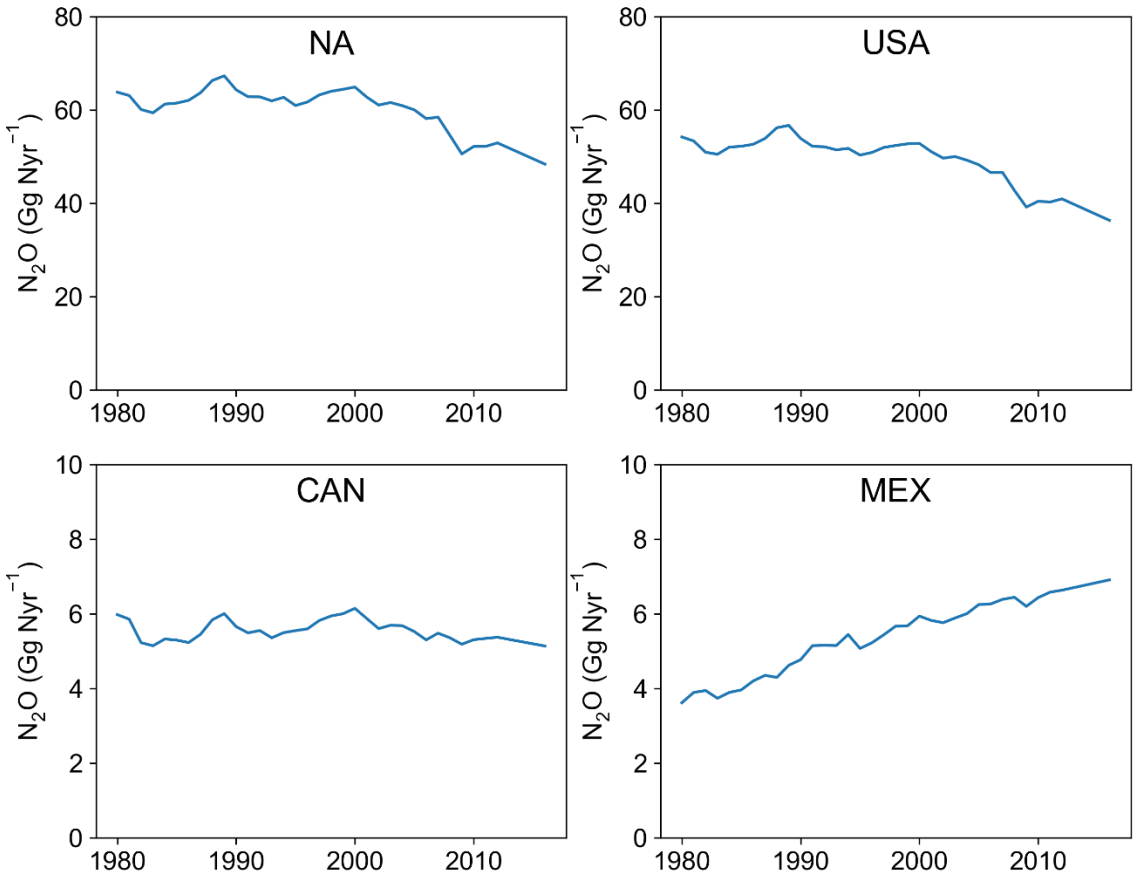


**Figure S5.** Indirect emissions from NDEP due to industrial activities estimated by EDGARv4.3.2.

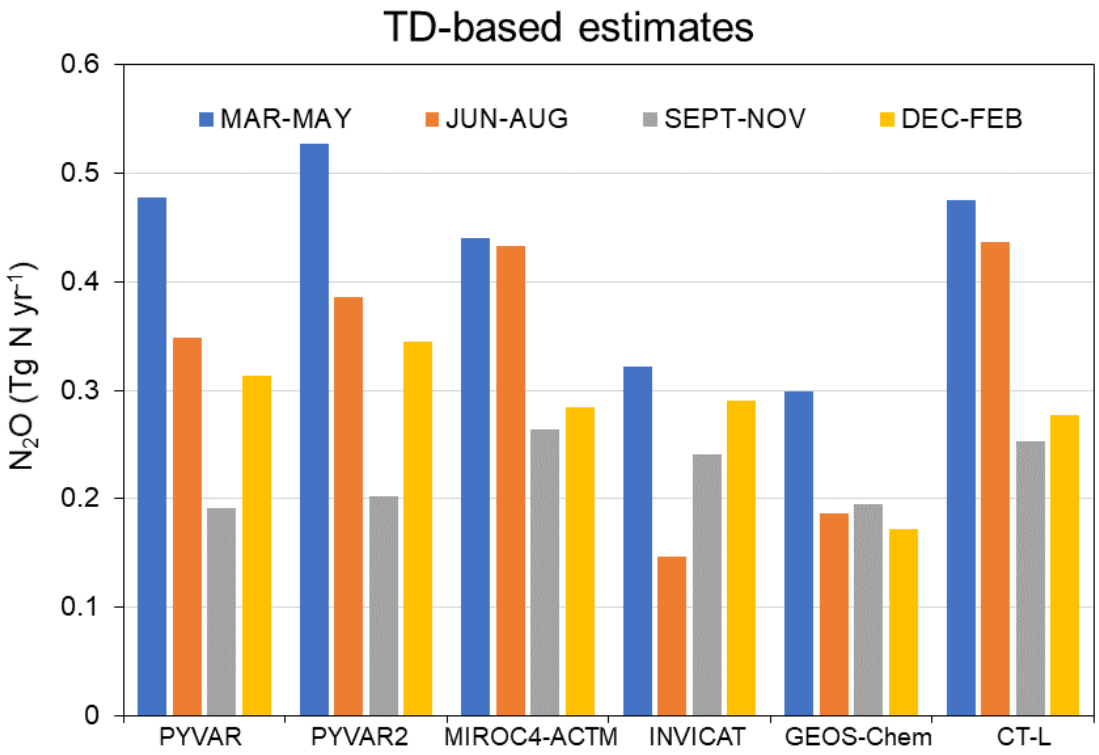


**Figure S6.** Seasonal total $N_2O$ fluxes from TD approaches over North America between 2008 and 2013. Five TD inversion models include PYVAR-CAMS, MIRCO4-ACTM, INVICAT, GEOS-Chem, and CT-L.

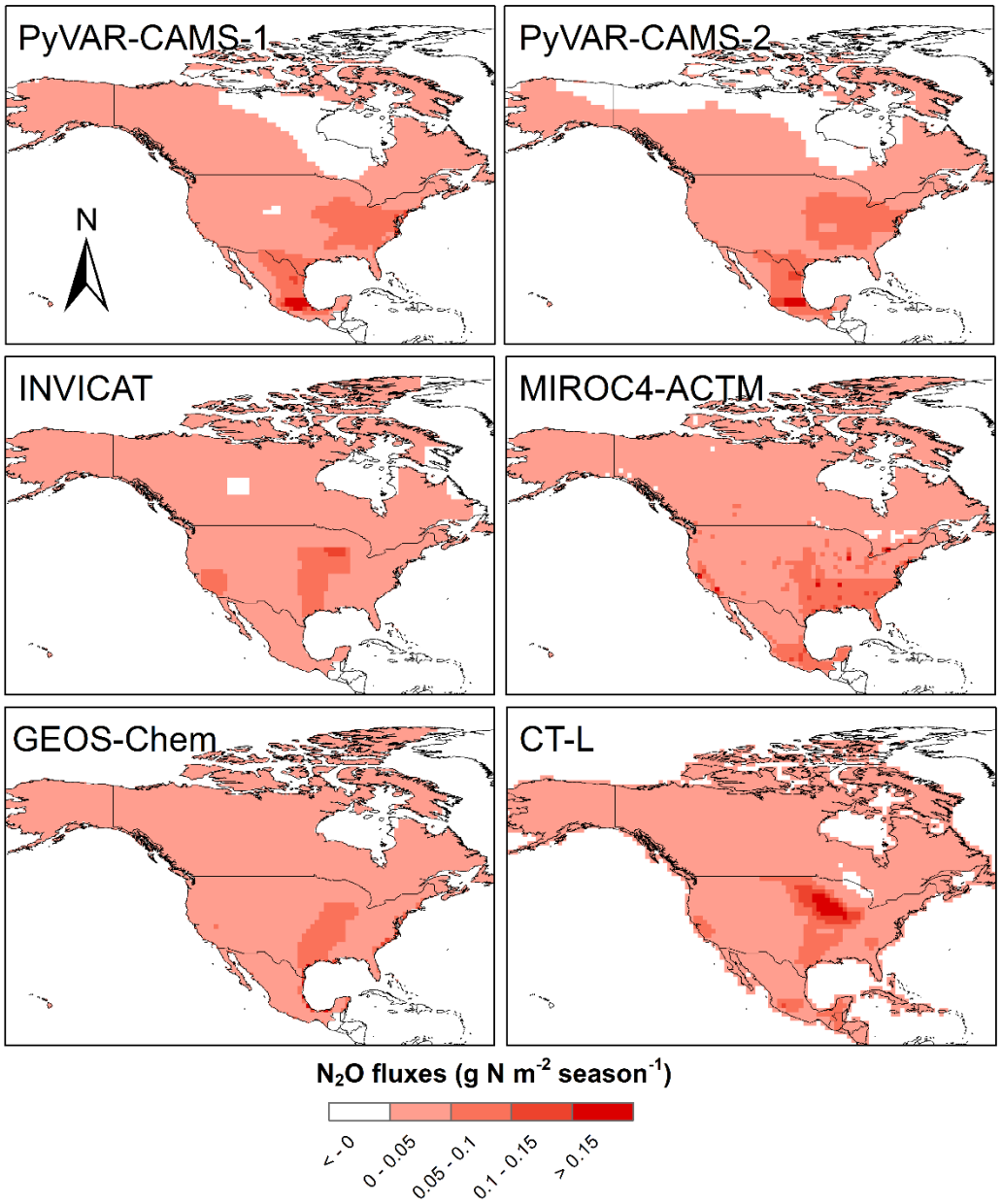


**Figure S7.** Comparison of spring $N_2O$ emissions (March, April, and May) by global inversion models with the estimate by the CT-L regional inversion model (Nevison et al., 2018) during 2008–2013. Global inversion models include PyVAR-CAMS-1 and CAMS-2, INVICAT, MIROC4-ACTM, and GEOS-Chem.

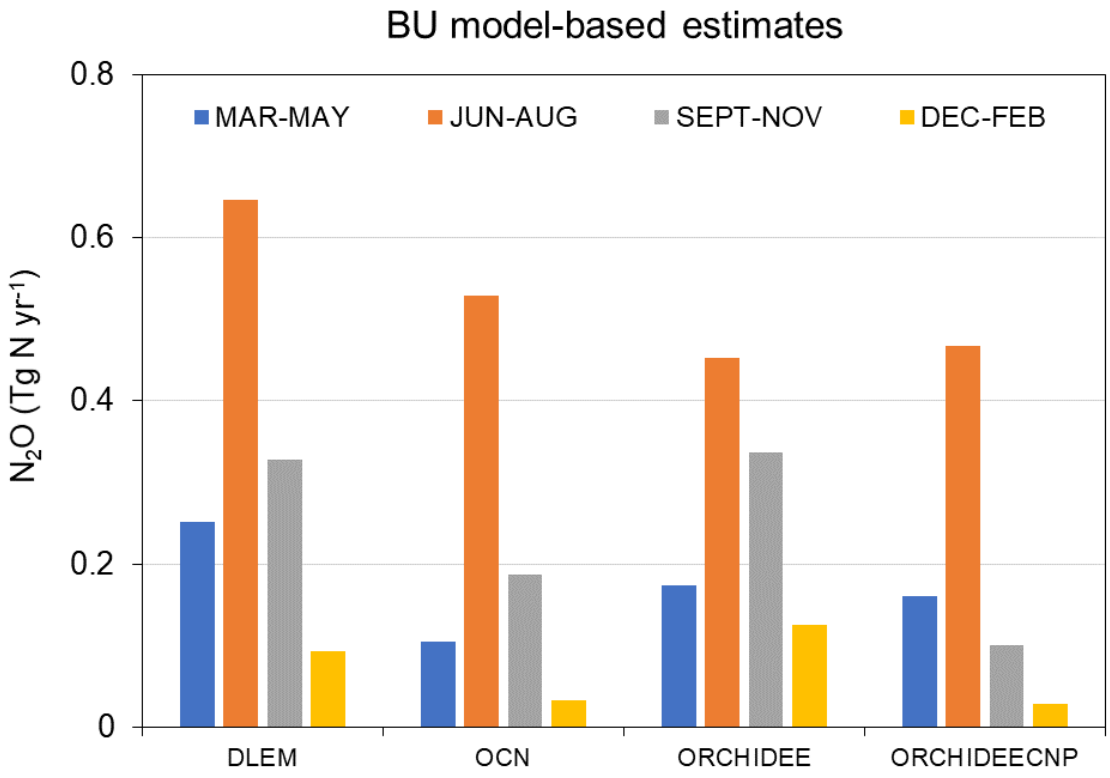


**Figure S8.** Seasonal cropland $N_2O$ fluxes from BU approaches over North America between 2007 and 2016. Four terrestrial biosphere models include DLEM, OCN, ORCHIDEE, and ORCHIDEE-CNP.

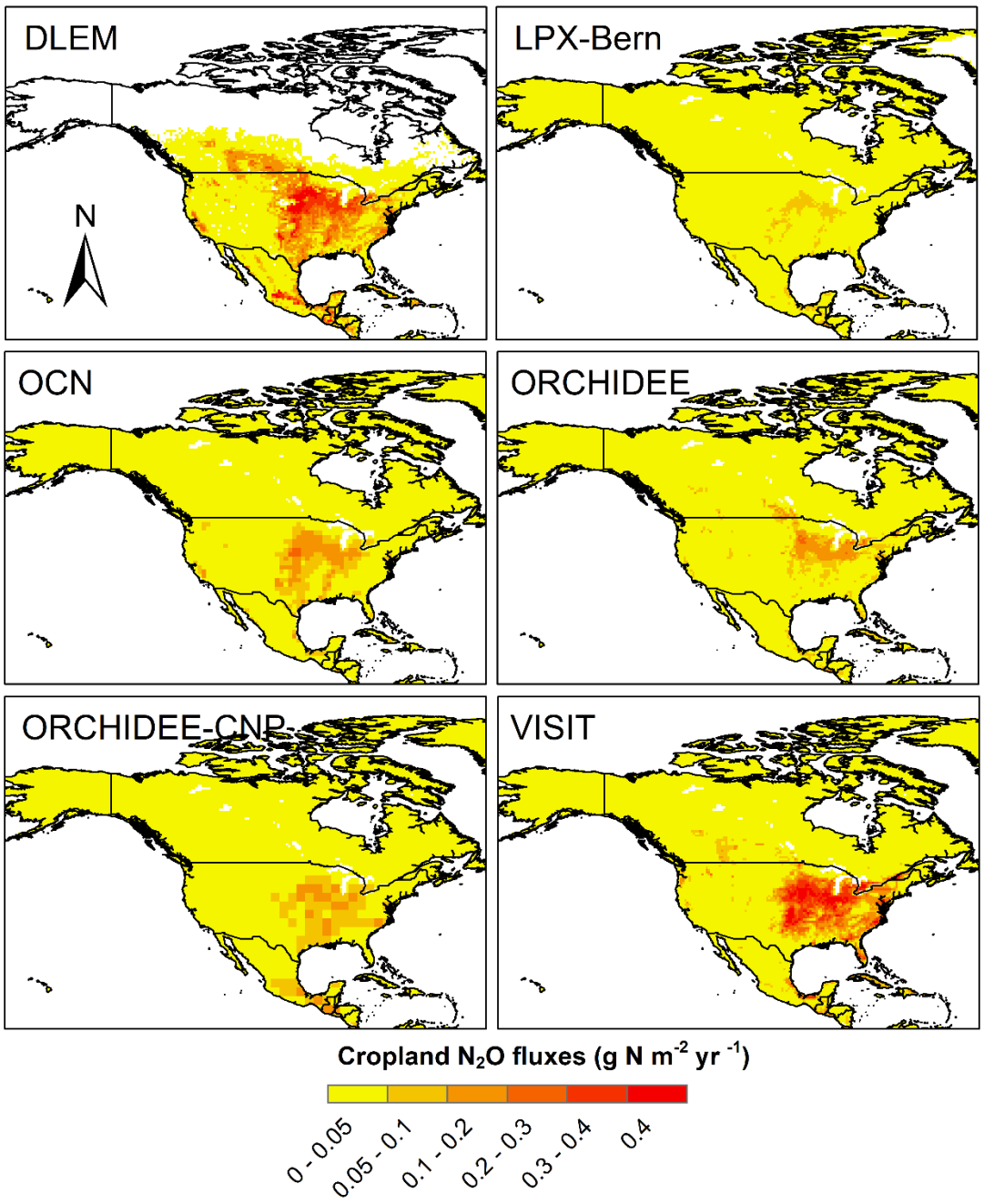


**Figure S9.** Spatial distribution of cropland $N_2O$ emissions by BU approaches. Six terrestrial biosphere models include DLEM, LPX-Bern, OCN, ORCHIDEE, ORCHIDEE-CNP, and VISIT.

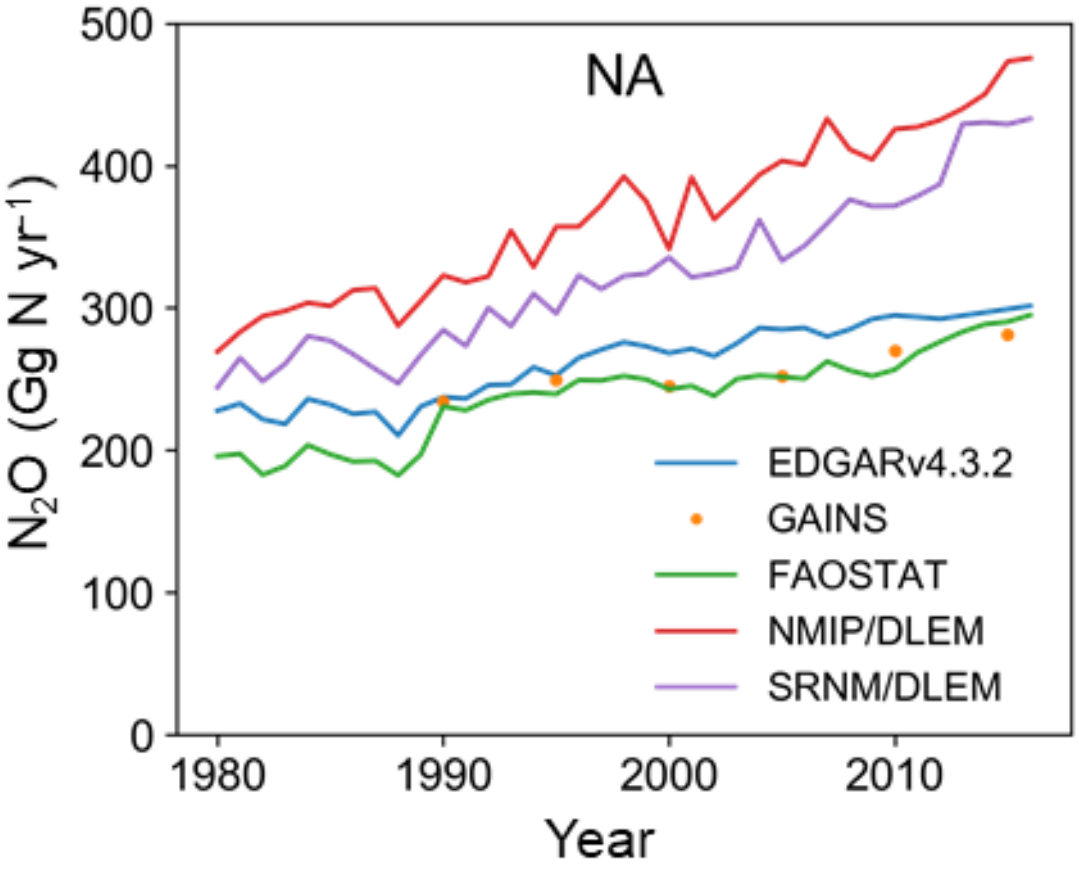


**Figure S10.** Direct emission from agricultural soils associated with mineral fertilizer, manure and crop residue inputs, and cultivation of organic soils based on EDGAR v4.3.2, GAINS, FAOSTAT, NMIP/DLEM, and SRNM/DLEM estimates in North America.

**Table S1.** Decadal changes in anthropogenic $N_2O$ sources over the past four decades over North America including the U.S., Canada, and Mexico.

| | | Decadal change (%) | | | |
|---|---|---|---|---|---|
| ***Anthropogenic sources*** | | USA | Canada | Mexico | North America |
| Direct emissions of N additions in the agricultural sector (Agriculture) | Direct soil emissions | 41 | 101 | 33 | 45 |
| | Manure left on pasture | -7 | 30 | 7 | -6 |
| | Manure management | 1 | 31 | 5 | 17 |
| | Aquaculture | N/A | N/A | N/A | 124 |
| | sub-total | **27** | **80** | **18** | **29** |
| Other direct anthropogenic sources | Fossil fuel and industry | -26 | -61 | 2283 | 1 |
| | Waste and waste water | 45 | 34 | 57 | 47 |
| | Biomass burning | | | | |
| | sub-total | **-22** | **-58** | **1168** | **3** |
| Indirect emissions from anthropoenic N additions | Inland waters, estuaries, coastal zones | 12 | 10 | 1 | 10 |
| | Atmospheric N deposition on land | -2 | 19 | 33 | 4 |
| | sub-total | **3** | **13** | **20** | **6** |
| Perturbed fluxes from climate/CO2/land cover change | Climate & $CO_2$ effect | 73 | 61 | 112 | 66 |
| | Post-deforestation pulse effect | -3 | -12 | -14 | -5 |
| | Long-term effect of reduced mature forest area | -7 | -1 | 19 | 0 |
| | sub-total | **18** | **11** | **137** | **9** |
| Anthropogenic total | | **7** | **-1** | **114** | **14** |

**Table S2.** Information on North American $N_2O$ measurement sites used in the global inversions from 1995 to 2016. CCG represents for discrete air samples from the National Oceanic and Atmospheric Administration Carbon Cycle Cooperative Global Air Sampling Network (NOAA); CSI represents for N2O measurements from the Commonwealth Scientific and Industrial Research Organization network (CSIRO); and AGA and CAT represent for N2O measurements from in-situ instruments in the Advanced Global Atmospheric Gases Experiment network (AGAGE) and the NOAA CATS network, respectively.

| **The global inversions: PyVAR-CAMS, INVICAT, GEOS-Chem** | | | | |
|---|---|---|---|---|
| **Sites** | **Latitude (°)** | **Longitude (°)** | **Altitude (m)** | **Type (FM: flask; CM: continuous)** |
| ALT_CCG | 82.45 | -62.52 | 205 | FM |
| ALT_CSI | 82.45 | -62.52 | 210 | FM |
| BAO_CCG | 40.05 | -105.01 | 1884 | FM |
| BRW_CAT | 71.32 | -156.61 | 11 | CM |
| BRW_CCG | 71.32 | -156.61 | 13 | FM |
| CBA_CCG | 55.21 | -162.72 | 25 | FM |
| ESP_CSI | 49.38 | -126.55 | 39 | FM |
| HSU_CCG | 41.05 | -124.73 | 7.6 | FM |
| KEY_CCG | 25.67 | -80.2 | 6 | FM |
| KUM_CCG | 19.52 | -154.82 | 8 | FM |
| LEF_CCG | 45.93 | -90.27 | 868 | FM |
| LLB_CCG | 54.95 | -112.45 | 546 | FM |
| MEX_CCG | 18.98 | -97.31 | 4469 | FM |
| MID_CCG | 28.22 | -177.37 | 11 | FM |
| MLO_CAT | 19.54 | -155.58 | 3397 | CM |
| MLO_CCG | 19.53 | -155.58 | 3402 | FM |
| MLO_CSI | 19.53 | -155.58 | 3397 | FM |
| MVY_CCG | 41.33 | -70.51 | 12 | FM |
| MWO_CCG | 34.22 | -118.06 | 1774 | FM |
| NWR_CAT | 40.05 | -105.58 | 3526 | CM |
| NWR_CCG | 40.05 | -105.58 | 3526 | FM |
| PTA_CCG | 38.95 | -123.73 | 22 | FM |
| SCT_CCG | 33.41 | -81.83 | 420 | FM |
| SGP_CCG | 36.62 | -97.48 | 374 | FM |
| SHM_CCG | 52.72 | 174.1 | 28 | FM |
| STR_CCG | 37.75 | -122.45 | 370 | FM |
| THD_AGA | 41.05 | -124.15 | 107 | CM |
| THD_CCG | 41.05 | -124.15 | 112 | FM |
| UTA_CCG | 39.9 | -113.72 | 1332 | FM |
| WBI_CCG | 41.72 | -91.35 | 621 | FM |
| WGC_CCG | 38.26 | -121.49 | 483 | FM |
| **The global inversion: MIROC4-ACTM** | | | | |
| **Sites** | **Latitude (°)** | **Longitude (°)** | **Altitude (m)** | **Type (FM: flask)** |
| BRW_CCG | 71.32 | -156.61 | 11 | FM |
| CBA_CCG | 55.21 | -162.72 | 21.34 | FM |
| KUM_CCG | 19.52 | -154.82 | 3 | FM |
| KEY_CCG | 25.67 | -80.16 | 1 | FM |
| NWR_CCG | 40.05 | -105.59 | 3523 | FM |

**Table S3.** Information on North American $N_2O$ measurement sites used in the CT-L regional inversion from 2007 to 2015 (Modified from Nevison et al., 2018).

| Site | Latitude (°) | Longitude (°) | Altitude m agl (*asl) | Number of Measurements | Data Period |
|---|---|---|---|---|---|
| ***Surface Sites*** | | | | | |
| AMT | 45.0 | -68.7 | 107 | 1460 | 1/07-12/15 |
| BAO | 40.1 | -105.0 | 300 | 2880 | 8/07-12/15 |
| BMW | 32.3 | -64.9 | 30 | 341 | 1/07-12/15 |
| BRW | 71.3 | -156.6 | 17 | 933 | 1/07-12/15 |
| CBA | 55.2 | -162.7 | 36 | 656 | 1/07-12/15 |
| CRV | 65.0 | -147.6 | 32 | 824 | 10/11-12/15 |
| HSU | 41.0 | -124.3 | 8 | 72 | 5/08-12/15 |
| INX | 39.6 to 39.9 | -86.4 to -85.7 | 156 to 225 | 1168 | 10/10-12/15 |
| KEY | 25.7 | -80.2 | 5 | 394 | 1/07-12/15 |
| LEF | 45.9 | -90.3 | 244 or 396 | 3138 | 1/07-12/15 |
| LLB | 55.0 | -112.5 | 48 | 193 | 1/08-2/13 |
| MBO | 44.0 | -121.7 | 11 | 629 | 10/11-5/14 |
| MEX | 19.0 | -97.3 | 4469* | 282 | 1/09-12/15 |
| MLS | 39.5 to 40.6 | -110.2 to -104.5 | 0 to 13 | 289 | 6/08-7/08 and 6/11-6/12 |
| MWO | 34.2 | -118.1 | 1774* | 2040 | 4/10-12/15 |
| NWR | 40.0 | -105.6 | 3526* | 730 | 1/07-12/15 |
| POC | 10 to 35 | -145 to -118 | 20 | 258 | 1/07-1/12 |
| SCT | 33.4 | -81.8 | 305 | 1867 | 8/08-12/15 |
| SGP | 36.6 | -97.5 | 60 | 452 | 1/07-12/15 |
| STR | 37.8 | -122.5 | 486* | 4036 | 10/07-12/15 |
| THD | 41.0 | -124.2 | 5 | 453 | 1/07-12/15 |
| UTA | 39.9 | -113.7 | 5 | 333 | 1/07-12/15 |
| WBI | 41.7 | -91.4 | 379 | 2876 | 6/07-12/15 |
| WGC | 38.3 to 39.3 | -121.5 | 91 | 2037 | 9/07-12/15 |
| WKT | 31.3 | -97.3 | 5, 122 or 457 | 2427 | 1/07-12/15 |
| ***Aircraft Sites*** | | | | | |
| ACG | 57.0 to 76.6 | -169.7 to -131.8 | 883 to 7969 | 1382 | 6/09-9/15 |
| CAR | 40.1 to 40.9 | -105.2 to -104.1 | 665 to 6658 | 2246 | 1/07-12/15 |
| CMA | 38.4 to 39.0 | -76.5 to -74.1 | 284 to 7422 | 1858 | 1/07-12/15 |
| DND | 47.2 to 48.5 | -99.5 to -96.2 | 138 to 7002 | 1202 | 1/07-12/15 |
| ESP | 49.3 to 49.6 | -126.6 to -125.7 | 314 to 5149 | 2432 | 1/07-12/15 |
| ETL | 53.9 to 54.6 | -105.3 to -104.4 | 463 to 6165 | 2180 | 1/07-12/15 |
| HIL | 39.9 to 40.2 | -88.1 to -87.7 | 727 to 7549 | 1642 | 1/07-12/15 |
| LEF | 45.7 to 46.1 | -90.4 to -89.9 | 160 to 3250 | 2133 | 1/07-12/15 |
| MLS | 32.1 to 48.8 | -112.2 to -96.1 | 2 to 3390 | 760 | 2/12-10/15 |
| NHA | 42.8 to 43.1 | -70.7 to -70.3 | 321 to 7300 | 2241 | 1/07-12/15 |
| PFA | 64.1 to 65.9 | -151.1 to -146.0 | 2343 to 6467 | 2342 | 1/07-12/15 |
| SCA | 32.5 to 33/9 | -79.8 to -79.3 | 332 to 7861 | 1888 | 1/07-12/15 |
| THD | 40.9 to 41.6 | -124.4 to -123.9 | 311 to 7901 | 1236 | 1/07-12/15 |
| TGC | 27.4 to 27.9 | -97.0 to -96.5 | 317 to 7893 | 1434 | 1/07-12/15 |
| WBI | 41.6 to 42.5 | -91.9 to -91.1 | 372 to 6372 | 1376 | 1/07-12/15 |

**Table S4.** Overview of the global and regional inversion frameworks.

| | Name | Method | ACTM horizontal resolution | Ocean prior |
|---|---|---|---|---|
| Global inversion models | INVICAT | 4D-Var | 5.625°×5.625° | 1 (high) |
| | PyVAR-CAMS-1 | 4D-Var | 3.75°×1.875° | 1 (high) |
| | PyVAR-CAMS-2 | | | 2 (low) |
| | MIROC4-ACTM | Bayesian analytical | 2.8°×2.8° | 3 (low) |
| | GEOS-Chem | 4D-Var | 5°×4° | 2 (low) |
| Regional inversion model | CT-L | Bayesian analytical | 1°×1° | NA |

**References**


Beusen, A. H., Bouwman, A. F., Van Beek, L. P., Mogollón, J. M., & Middelburg, J. J. (2016). Global riverine N and P transport to ocean increased during the 20th century despite increased retention along the aquatic continuum. *Biogeosciences, 13*(8), 2441-2451.

Bouwman, A. F., Beusen, A., Overbeek, C., Bureau, D., Pawlowski, M., & Glibert, P. (2013). Hindcasts and future projections of global inland and coastal nitrogen and phosphorus loads due to finfish aquaculture. *Reviews in Fisheries Science, 21*(2), 112-156.

Bouwman, A. F., Pawłowski, M., Liu, C., Beusen, A. H., Shumway, S. E., Glibert, P., & Overbeek, C. (2011). Global hindcasts and future projections of coastal nitrogen and phosphorus loads due to shellfish and seaweed aquaculture. *Reviews in Fisheries Science, 19*(4), 331-357.

FAO, 2021. FAOSTAT Emissions database, http://www.fao.org/faostat/en/#data/GT, FAO, Rome, Italy.

Janssens-Maenhout, G., Crippa, M., Guizzardi, D., Muntean, M., Schaaf, E., Dentener, F., et al. (2019). EDGAR v4.3.2 Global Atlas of the three major greenhouse gas emissions for the period 1970–2012. *Earth System Science Data, 11*(3), 959-1002. https://www.earth-syst-sci-data.net/11/959/2019/

Lauerwald, R., Regnier, P., Figueiredo, V., Enrich-Prast, A., Bastviken, D., Lehner, B., et al. (2019). Natural lakes are a minor global source of $N_2O$ to the atmosphere. *Global Biogeochemical Cycles, 33*, 1564-1581.

Maavara, T., Lauerwald, R., Laruelle, G. G., Akbarzadeh, Z., Bouskill, N. J., Van Cappellen, P., & Regnier, P. (2019). Nitrous oxide emissions from inland waters: Are IPCC estimates too high? *Global change biology, 25*(2), 473-488.

MacLeod, M., Hasan, M. R., Robb, D. H. F., & Mamun-Ur-Rashid, M. (2019). *Quantifying and mitigating greenhouse gas emissions from global aquaculture*. Retrieved from Rome.

Nevison, C., Andrews, A., Thoning, K., Dlugokencky, E., Sweeney, C., Miller, S., et al. (2018). Nitrous Oxide Emissions Estimated With the CarbonTracker-Lagrange North American Regional Inversion Framework. *Global Biogeochemical Cycles, 32*(3), 463-485.

Tian, H. Q., Yang, J., Xu, R. T., Lu, C. Q., Canadell, J. G., Davidson, E. A., et al. (2019). Global soil nitrous oxide emissions since the preindustrial era estimated by an ensemble of terrestrial biosphere models: Magnitude, attribution, and uncertainty. *Global change biology, 25*(2), 640-659. <Go to ISI>://WOS:000456028900021

Tubiello, F., Cóndor-Golec, R., Salvatore, M., Piersante, A., Federici, S., Ferrara, A., et al. (2015). *Estimating greenhouse gas emissions in agriculture: a manual to address data requirements for developing countries*. Retrieved from Rome

Van Der Werf, G. R., Randerson, J. T., Giglio, L., Van Leeuwen, T. T., Chen, Y., Rogers, B. M., et al. (2017). Global fire emissions estimates during 1997-2016. *Earth System Science Data, 9*, 697-720.

Wang, Q., Zhou, F., Shang, Z., Ciais, P., Winiwarter, W., Jackson, R. B., et al. (2019). Data-driven estimates of global nitrous oxide emissions from croplands. *National Science Review, 00*, 1-12.

Winiwarter, W., Höglund-Isaksson, L., Klimont, Z., Schöpp, W., & Amann, M. (2018). Technical opportunities to reduce global anthropogenic emissions of nitrous oxide. *Environmental Research Letters, 13*(1), 014011.

Yao, Y., Tian, H., Shi, H., Pan, S., Xu, R., Pan, N., & Canadell, J. G. (2020). Increased global nitrous oxide emissions from streams and rivers in the Anthropocene. *Natural Climate Change, 10*(2), 138-142.